On Possible Locations for a GBT Quadrant Detector
Roger D. Norrod
January 4, 1996

1.0 Introduction

Development and installation of a "Quadrant Detector" (QD) system on the GBT is included in the goals and budget of the Metrology group. Some preliminary development of a prototype is described in a memo by M. Valente which, for convenience, is attached as Appendix A. In concept, the QD system will include a laser package attached to a relatively rigid portion of the antenna, and a detector package attached to a second portion of the structure. The detector is to measure the displacements of its supporting structure relative to the "stationary" laser beam. An obvious application of such a measurement system on the GBT is to measure the dynamic displacements of the feedarm to assist in estimating rapid changes in the antenna beam pointing error.

This memo is a first cut at considering some possible locations for the QD laser and detector, and how the choice of those locations sets design requirements on the QD components. Four possible nodes for locating a laser are considered; three in the backup box structure and one on a surface actuator. Only one detector location is considered as of yet, on the Receiver Room. The main aspects considered are the extent of relative motions of the laser and detector locations over the range of antenna elevations, effects of tilting of the laser nodes, and the ability to view the upper feedarm from the laser nodes in the backup structure.

2.0 Computer Programs

A program was written to assist in studying how the antenna structural nodes move versus elevation. The program uses calls to the functions "get_index" and "get_node_data" provided by D. Wells and described in GBT Memo 124. The executable and source code for the program described below are available in the Green Bank directory ~rnorrod/Gbt/Model/Wells_model/gbt_tipping/. Also available in this directory are the complete output files for all the arrangements considered in this memo, parts of which are reproduced in this memo.

The program, "qd" (source file qd.c), prompts the user for four input parameters:

> A QD Rigging Elevation - This is the antenna elevation at which the QD components would be aligned. Part of the output data of qd is expressed relative to the locations at the QD rigging elevation.

Laser Node and Detector Node numbers.

A y/n flag that causes the program to include or not include effects of laser node tilts in its output. This is useful for separating the effects of node displacements from that of laser tilt.

The program then writes its output to the file "qd.txt" and exits.

An example output file is given in Appendix B. The first portion gives the grid coordinates of the laser and detector nodes (in the Elevation coordinate system of C35102M081), and the node displacements and tilts at the QD rigging elevation. Next, the length of the laser beam (the 3D distance between the laser and detector nodes) at the rigging elevation is given. Two tables follow in the output, giving the absolute positions of the laser and detector nodes at elevations between 0 and 90 degrees. Also given in these two tables is the node position relative to its position at the QD rigging elevation.

The third table output by qd gives the "Laser Beam Tip Position" as a function of elevation. The sequence of calculations used at each elevation to produce these coordinates follow. The laser beam is taken to be a vector of constant length over the range of elevations. This vector is rotated by the three tilt angles of the laser node, and is then displaced by the laser node displacements. The resulting coordinates of the vector tip is output, in both the absolute elevation coordinate system, and relative to the rigging elevation position. (The laser beam is not truly of fixed length due to movement of the detector node away from or toward the laser node. Not taking into account this effect will produce an error in the calculated beam tip position. It is felt that the magnitude of this error is not important for the purposes of this memo, but is an area where the calculations in qd need to be refined.)

For the final two output tables, a new coordinate system (L2) is formed. A set of axes, aligned with the elevation coordinate system, is first placed at the laser node. The axes are then rotated about the Z axis to align the new Y axis with the projection of the laser vector onto the X-Y plane. The axes are then rotated about the X axis to align the new Z axis with the laser beam vector. As a check of this process, the coordinates of the laser beam tip in the L2 system are output in the next-to-last table. The X and Y components should be zero and the Z component should be constant and equal to the laser beam length at the rigging angle.

The final table output by qd is probably of the most use. It gives the coordinates of the detector node expressed in the L2 coordinate system. The QD will detect X and Y components of these positions and will be insensitive to the Z component. The mechanical displacement system built into the detector package must have travel range at least sufficient to cover the extent of the XY detector displacements in order to track the laser beam as the antenna elevation changes.

3.0 Discussion of Results

Four cases were considered for location of the laser: Node 1000 - the center of the elevation axle; Node 10030 - at the top of the box structure directly over node 1000; Node 10230 - at the top of the box where the encoder backshaft terminates (see below); and Node 700017 - the top of the surface actuator which sits on Hoop 17 at the symmetric plane. For all cases, the detector node is taken to be 40710 - at the top front center edge of the receiver room, and the QD rigging angle is taken at 44 degrees. Figure 1 shows an elevation view of case 2. Figure 2 shows a perspective cut-away view of the box and backup structure identifying the locations of nodes 1000, 10030, and 10230. Figure 3 is taken from the Loral Tech Memo 42, showing the elevation backshaft - a tube which turns the elevation encoder. This backshaft terminates at the bottom and top (at node 10230) of the box structure, and is independent of the el axle main structure.

3.1 Laser at Node 1000

For the first case considered, Figure 4 shows a perspective Autocad view from node 1000; node 40710 is in the center of the image. Figure 5 shows the view as presented by the Visualization Workstation, where the backup and box structure members were represented by 4 inch diameter tubes. For Figure 5, the point of view was moved 30 inches left of node 1000 to get out from under the R0 truss. The feedarm cannot be seen in Figure 5 because the panels are opaque, but the detector at 40710 would again lie in the center of the image. The laser would go through the panel just below Hoop 17, and although there is a diagonal backup structure beam cutting through the middle of that panel as viewed from this location, there probably is adequate viewing. Table 1 gives the detector position for this case, in L2 coordinates as output by qd. It can be seen from this table that almost 8 inches of detector travel in the L2-Y direction would be required. For this case, the laser beam at the rigging elevation is 3015 inches long.

Table 1
Detector Position in L2 for Laser at Node 1000

EL	X	Absolute Y	Z
0	-0.000	-3.705	3013.147
5	-0.000	-3.353	3013.246
10	-0.000	-2.977	3013.382
15	-0.000	-2.579	3013.553
20	-0.000	-2.162	3013.758
25	-0.000	-1.730	3013.995
30	-0.000	-1.284	3014.262
35	-0.000	-0.830	3014.558
40	-0.000	-0.370	3014.879
45	-0.000	0.092	3015.225
50	-0.000	0.553	3015.591
55	-0.000	1.009	3015.976
60	-0.000	1.457	3016.376
65	-0.000	1.893	3016.789
70	-0.000	2.313	3017.210
75	-0.000	2.716	3017.638
80	-0.000	3.097	3018.068
85	-0.000	3.453	3018.498
90	-0.000	3.783	3018.923

3.2 Laser at Node 10030

For the second case considered, Figure 6 shows a perspective Autocad view from node 10030; node 40710 is in the center of the image. Figure 7 shows the view as presented by the Visualization Workstation, where the backup and box structure members were represented by 4 inch diameter tubes. For Figure 7, the point of view was moved 30 inches left of node 10030 to get out from under the R0 truss. The feedarm cannot be seen in Figure 7 because the panels are opaque, but the detector at 40710 would again lie in the center of the image. The laser would go through the panel just above Hoop 17, and although the laser beam directed at 40710 comes quite near the panel edge, there probably is adequate viewing. Figure 8 shows a Visualization view in which a clipping plane is set near the plane of the panels such that it is possible to visualize the upper feedarm. Table 2 gives the detector position for the laser at 10030, in L2 coordinates as output by qd. It can be seen from this table that almost 12 inches of detector travel in the L2-Y direction would be required to track the laser beam motion due to gravitational deformations over

the range of antenna elevations. For this case, the laser beam at the rigging elevations is 2837 inches long.

As mentioned earlier, it is possible to cause the program qd to perform its calculations ignoring effects of tilts at the laser node. Figure 9 shows the L2-Y component of detector position for the laser at 10030, with and without the laser tilt effect. It can be seen that the laser tilt increases the required travel range by approximately 1.6 inches. It is interesting to note that the structural model reports that the tilts about the X-axis of node 1000 is the opposite sense to that of node 10030, meaning the laser tilt at node 1000 tends to *reduce* the tracking range needed.

The program qd can also be used to estimate the size of a hole which would be required in a surface panel to view a particular spot on the feedarm, by determining the relative motion between a particular laser node and a surface panel support node near where the laser beam passes. Table 3 gives such data, for the laser at 10030. It can be seen that a 1-2 inch diameter hole in the surface panel should be sufficient.

Table 2
Detector Position in L2 for Laser at Node 10030

EL	X	Y	Z
		Absolute	
0	-0.000	-5.492	2834.908
5	-0.000	-4.989	2835.021
10	-0.000	-4.444	2835.171
15	-0.000	-3.863	2835.357
20	-0.000	-3.249	2835.577
25	-0.000	-2.606	2835.830
30	-0.000	-1.941	2836.113
35	-0.000	-1.258	2836.424
40	-0.000	-0.562	2836.762
45	-0.000	0.141	2837.123
50	-0.000	0.846	2837.505
55	-0.000	1.549	2837.905
60	-0.000	2.242	2838.320
65	-0.000	2.922	2838.746
70	-0.000	3.583	2839.181
75	-0.000	4.219	2839.621
80	-0.000	4.827	2840.062
85	-0.000	5.401	2840.503
90	-0.000	5.937	2840.938

Table 3
Detector Position in L2
Laser at 10030
and Detector at Surface Actuator 700017
to Estimate Panel Hole Size for Laser Beam

| | | Absolute | |
EL	X	Y	Z
0	-0.000	-0.330	491.201
5	-0.000	-0.305	491.197
10	-0.000	-0.276	491.194
15	-0.000	-0.244	491.191
20	-0.000	-0.208	491.188
25	-0.000	-0.169	491.186
30	-0.000	-0.128	491.185
35	-0.000	-0.084	491.183
40	-0.000	-0.038	491.183
45	-0.000	0.010	491.183
50	-0.000	0.059	491.183
55	-0.000	0.109	491.184
60	-0.000	0.160	491.185
65	-0.000	0.211	491.187
70	-0.000	0.261	491.189
75	-0.000	0.312	491.192
80	-0.000	0.361	491.195
85	-0.000	0.409	491.199
90	-0.000	0.456	491.203

3.3 Laser at Node 10230

For the third laser location considered, Figure 10 shows a perspective Autocad view from node 10230; node 40710 is in the center of the image. As mentioned earlier, 10230 is the top box node at which the encoder backshaft terminates and is well off the structure plane of symmetry. Figure 11 shows the view as presented by the Visualization Workstation, where the backup and box structure members were in this case represented by 10 inch diameter tubes. A clipping plane is set near the plane of the panels such that it is possible to visualize the upper feedarm. Table 4 gives the detector position for the laser at 10230, in L2 coordinates as output by qd. It can be seen from this table that almost 10 inches of detector travel in the L2-Y direction, and almost 5 inches in the L2-X direction, would be required to track the laser beam motion due to

gravitational deformations over the range of antenna elevations. Figure 12 shows a view looking down onto the GBT main reflector. The surface actuators which are highlighted surround the surface panel through which the QD laser beam would shine in this case.

Table 4
Detector Position in L2 for Laser at Node 10230

EL	X	Absolute Y	Z
0	3.279	-4.273	2872.767
5	2.865	-3.925	2872.856
10	2.455	-3.533	2872.982
15	2.052	-3.102	2873.145
20	1.659	-2.634	2873.344
25	1.278	-2.134	2873.577
30	0.914	-1.604	2873.841
35	0.568	-1.049	2874.136
40	0.243	-0.473	2874.459
45	-0.058	0.120	2874.807
50	-0.333	0.724	2875.178
55	-0.580	1.337	2875.569
60	-0.797	1.952	2875.977
65	-0.982	2.565	2876.399
70	-1.134	3.172	2876.832
75	-1.252	3.768	2877.272
80	-1.334	4.348	2877.716
85	-1.380	4.908	2878.160
90	-1.390	5.444	2878.602

3.4 Laser On Surface at Node 700017

For the fourth possible laser location, the placement of the QD laser on top of one of the surface actuators was considered. The actuator on the plane of symmetry at hoop 17 was selected (node 700017). Table 5 gives the detector position for the laser at this location, in L2 coordinates as output by qd. It can be seen for this case that approximately 7 inches of detector travel in the L2-Y direction would be required to track the laser beam motion over the range of antenna elevations. For this case, the laser beam at the rigging elevation is 2346 inches long.

Table 5
Detector Position in L2 for Laser at Node 700017

EL	X	Absolute Y	Z
0	-0.000	-3.386	2343.751
5	-0.000	-3.049	2343.866
10	-0.000	-2.694	2344.019
15	-0.000	-2.323	2344.206
20	-0.000	-1.938	2344.427
25	-0.000	-1.543	2344.680
30	-0.000	-1.140	2344.964
35	-0.000	-0.733	2345.275
40	-0.000	-0.325	2345.613
45	-0.000	0.081	2345.973
50	-0.000	0.482	2346.354
55	-0.000	0.875	2346.752
60	-0.000	1.258	2347.165
65	-0.000	1.626	2347.589
70	-0.000	1.977	2348.021
75	-0.000	2.309	2348.458
80	-0.000	2.619	2348.897
85	-0.000	2.905	2349.333
90	-0.000	3.164	2349.765

4.0 Summary

From these results, it seems that it would be possible to place the QD laser at any of the locations considered and achieve adequate viewing of a target on the upper feedarm. It will be necessary to calibrate out the large displacements due to gravity over elevation; hopefully these will be quite repeatable. To keep this calibration as simple as possible, it probably would be preferrable to keep both the laser and the detector near the plane of symmetry, ruling out the use of node 10230.

The results illustrate the sensitivity of the system to tilts at the laser; because the length of the laser beam is on the order of 3000 inches, each milliradian of laser tilt equates to about 3 inches of movement of the beam at the detector. Since the tilt of node 1000 tends to cancel the relative displacements, the Y tracking calculated for node 1000 is less than that for the laser at node 10030, despite the longer beam length. However, of the locations in the box structure considered, placing the laser near node 10030 rather than node 1000 seems preferrable because the encoder backshaft moves largely independently of the el axle.

Placing the QD laser at the primary surface, similar to the arrangement discussed in 3.4, seems worthy of serious consideration as well. Advantages include a shorter laser beam, and it would be possible to use the feedarm rangefinders to assist in calibration and monitoring of slow displacements of the laser relative to the detector. Disadvantages at such a location could include larger vibrations which would confuse the measurements.

Finally, because of the QD insensitivity to movements along the laser beam, the primary utility of any of the arrangements considered here would be to monitor displacements of the upper feedarm out of the plane of symmetry. This is the expected movement induced by the fundamental structural resonance mode.

Appendix A
Remote Laser Motion Tracker
Martin J. Valente

REMOTE LASER MOTION TRACKER

BY

MARTIN J. VALENTE

NATIONAL RADIO ASTRONOMY OBSERVATORY

beam. LVDTs on the translation stage then give the required X and Y displacement values. By using the detector in this nulling mode, highly linear and accurate performance will be obtained. The servo systems remain to be completed.

The system is made insensitive to ambient light changes by filtering the light input to the detector and modulating the laser beam.

Electronics

X - Y Error Signals

Location Close
to Subreflector

Drive Signals

Servo Controlled
X & Y translation stages

Reducer/Detector Assembly

α 60 m

Laser/Expander Assembly

Vertex
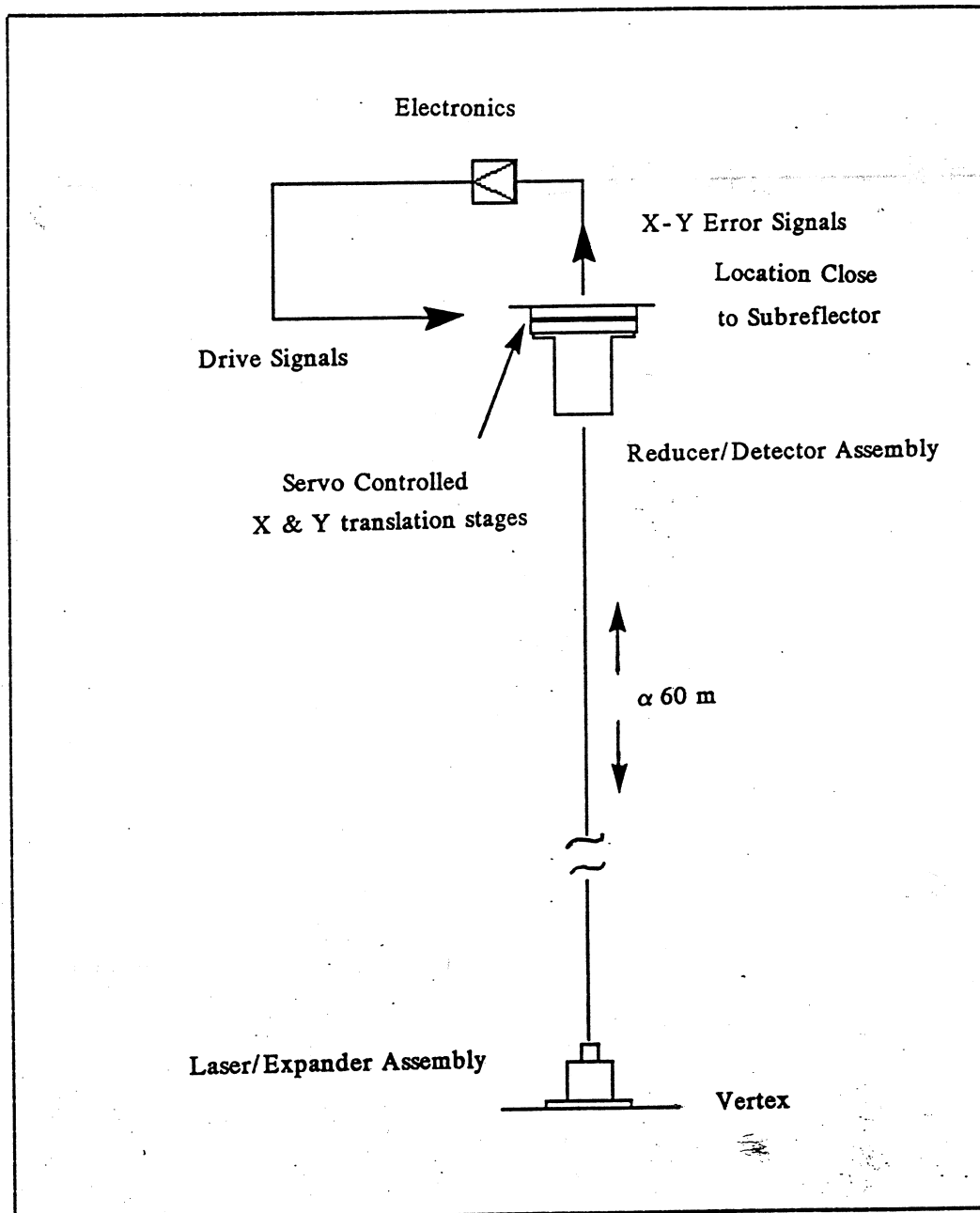
Figure 1. Monitoring Arm Movements on the GBT.

Gaussian Equation:

$$W(Z) = W_0 \left[1 + \left[\frac{Z\lambda}{\pi(W_0)^2} \right]^2 \right]^{\frac{1}{2}}$$

$W(Z)$ = beam radius

W_0 = beam waist

Z = distance from beam waist

Optimize by: $\dfrac{d\,W(Z)}{d\,W_0} = 0$

$$W_0 = \left[\frac{Z\lambda}{\pi} \right]^{\frac{1}{2}} = \text{optimum expanded beam waist}$$

W_0 expanded = 3.45 mm

Initial beam waist: 0.75 mm x 1.0 mm ; W_0 avg = 0.875 mm

$$\frac{W_0 \text{ expanded}}{W_0 \text{ avg}} = 3.95 = \text{Optimum magnification}$$

With W_0 = 0.75 mm W (50 m) = 4.98 mm

W_0 = 1.00 mm W (50 m) = 4.99 mm

Figure 2. Beam Expander Calculations

The reduction ratio of the beam reducer was set to yield high positional resolution. The formula used to calculate the resolution is:

δP = (spot dia - gap)/(2*SNR) [2]. The manufacturer of the quadrant detector specified a minimum spot size of 0.5mm diameter. The reduction ratio was determined so that the spot size was slightly above the manufacturer's minimum specification. The expanded beam diameter is 10mm going into the reducer, and therefore the reduction ratio was set to 1/16.67 so that the spot size is 0.6mm in diameter. This spot size then requires that the SNR be greater than 300 in order to resolve 1 micron on the detector. This SNR criterion is easily achievable.

The focal lengths of the lenses in the afocal system are: $f1 = 250$mm and $f2 = 15$mm. These lenses were readily available in BK7 with anti-reflection coatings to maximize the transmission through the system. The plano convex shape was chosen because of its good performance at infinite conjugate ratio and low cost. Furthermore, this lens shape exhibits near-minimum total transverse aberration and near zero coma when used off-axis. The precise spacing between the lenses was solved for using optical design software. The quadrant detector was placed at the exit pupil of the reducer optics, the exit pupil is a one to one mapping of the collecting optic in this system. By placing the detector at the exit pupil, this system will be insensitive to any angular variations in the incoming beam. Therefore, if the incident beam translates and tilts due to a cantilever effect, the detector will only sense the translation and the tilt will not produce a positional error. See figure 5 for the optical layout of the reducer.
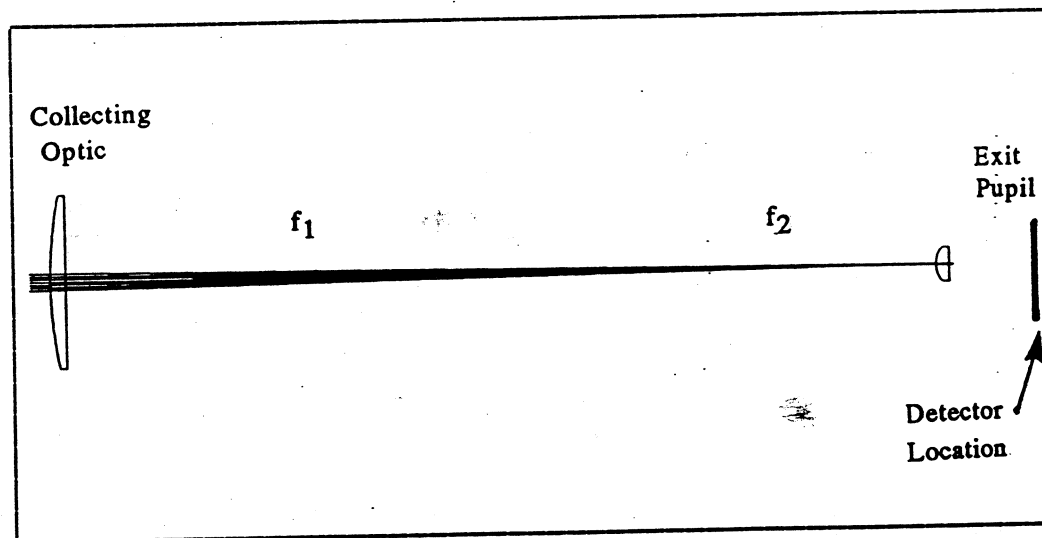

Figure 5. Beam Reducer

The operation of the quadrant detector therefore limits the travel range of the spot to roughly twice the spot diameter (ignoring the gap between quadrants for a first order approximation). This could lead one to believe that the travel range of the incident beam can be increased by decreasing the beam reduction ratio and thereby increasing the spot size diameter on the detector. By studying the beam size through the system, we can see that the reduction ratio has no first order effect on the travel range. Let the variable B equal the diameter of the incident beam on the reducer, and the variable R equal the reduction ratio $f2/f1$. Then the spot diameter, S, is B*R. The travel range across the quadrant detector is twice the spot diameter, $D=2*S$. The travel range of the system is equal to the travel range, TR, of the center of the incident beam prior to entering the reducer optics. This range is determined by multiplying the detector travel range, D, by the reciprocal of the reduction ratio, $1/R$ (magnification). The resultant formula is: $TR = D/R = (2*S)/R = 2*(B*R)/R = 2*B$, which states that the travel range of the incident beam is not a function of the reduction ratio. Since the expanded beam diameter is 10mm, as determined by optimizing the divergence, the travel range of the incident beam is roughly 20mm. Since the travel range of the system is equal to the travel range of the center of the incident beam, the radius distance of the incident beam must be subtracted at each extreme of the incident beam travel range. This results in a system travel range equal to the diameter of the incident beam, $20mm - 10mm = 10mm$. See figure 7 for the incident beam travel range determination.

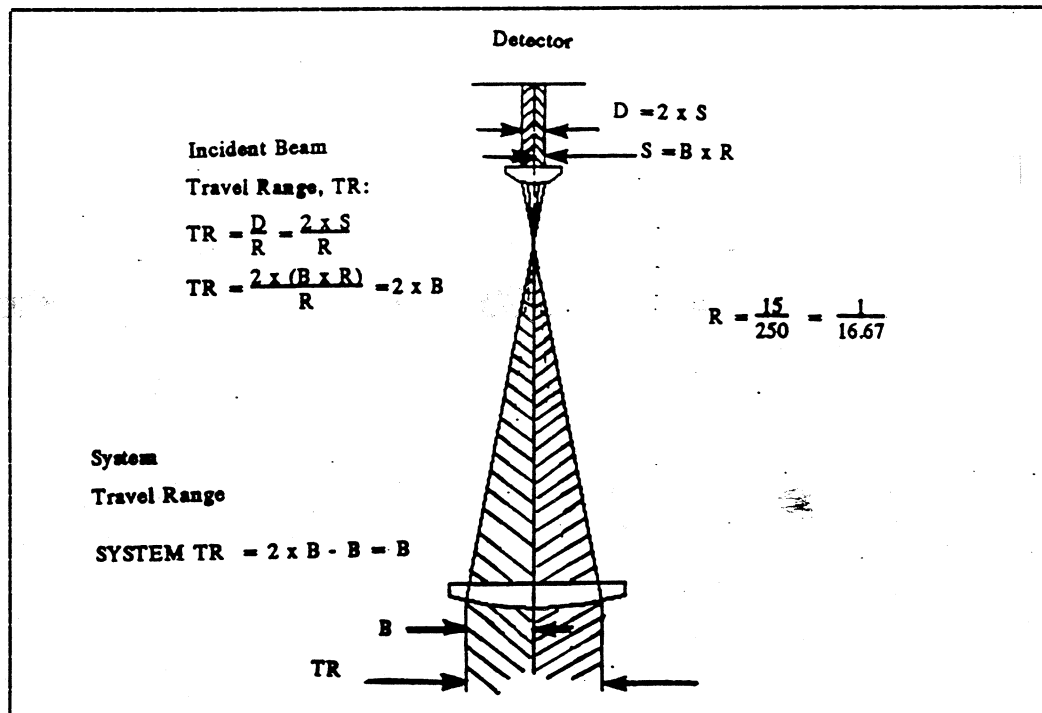Figure 7. Travel Range of Incident Beam

$$\delta P = \frac{S}{2 \times SNR}$$

for $SNR = 10^3$ and $S = 0.6$ mm $\left[R = \frac{1}{16.70} \right]$

$\delta P = 0.3 \mu m$

for $S = 1.0$ mm $\left[R = \frac{1}{10} \right]$

$\delta P = 0.5 \mu m$ **67 percent decrease**

$$TR = ((2 \times S) - .180mm) \times \frac{1}{R} - 10mm$$

for $R = \frac{1}{16.7}$ $S = 0.6$ mm

$TR = 17.0mm - 10mm = 7.0mm$

for $R = \frac{1}{10}$ $S = 1.0$ mm

$TR = 18.2mm - 10mm = 8.2mm$ **17 percent increase**

Figure 9. Resolution vs. Travel Range

ENVIRONMENTAL EFFECTS ON SYSTEM PERFORMANCE

The system is to be used outdoors, therefore precautions must be taken to filter out the effects of ambient light.

A laser line interference filter was placed in front of the reducer optics to filter out a 20nm region centered at 750nm (the incident beam wavelength). This was found to be a very effective way to block out most of the ambient light. In order to completely isolate the system, a combination of an ac-amplifier and a synchronous detector scheme was used in conjunction with modulating the diode laser beam. The circuitry will be discussed in detail in the electronics portion of this paper.

Another environmental consideration was the effect of the atmosphere on the laser beam propagation. Beam spreading due to turbulence was determined to be negligible. By the formula: $A = 2.01(\lambda^{-.2} \; 10E\text{-}8^{1.2} \; Z^{1.6}) = 4.4E\text{-}6$ meters, where A is the beam spread induced by turbulence [4]. Atmospheric absorption was also considered and found to be approximately 2 percent at 35 deg C, humidity 25
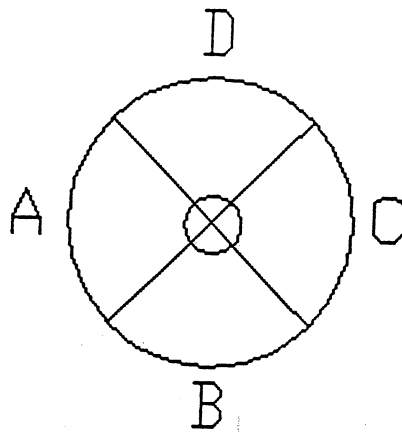
$$R = \frac{.35 \, A}{W}$$

(assume 10kΩ resistors)

Before fluctuation :

Quadrant A : $\phi_{incident} = 1 \, mW$

Current $= \phi R = 0.35 \, mA$

$V = (.35 \, mA)(10 \, k\Omega) = 3.5 \, V$

Quadrant C : $\phi_{incident} = 0.5 \, mW$

Current $= \phi R = 0.175 \, mA$

$V = (.175 \, mA)(10 \, k\Omega) = 1.75 \, V$

A - C = 1.75 V

$$\frac{A - C}{A + C} = 0.333$$

During fluctuation :

Quadrant A : $\phi_{incident} = 0.1 \, mW$

Current $= \phi R = .035 \, mA$

$V = (.035 \, mA)(10 \, k\Omega) = .35 \, V$

Quadrant C : $\phi_{incident} = .05 \, mW$

Current $= \phi R = .0175 \, mA$

$V = (.0175 \, mA)(10 \, k\Omega) = .175 \, V$

A - C = .175 V

$$\frac{A - C}{A + C} = 0.333$$

Figure 11. Intensity Fluctuations

ELECTRONICS

The schematic diagram for the circuit is shown in figure 12. The 555 multivibrator is used to modulate the laser diode and trigger the CMOS switches of the synchronous detector. The frequency of modulation was set at 1kHz to stay well below the maximum modulation specification of the laser diode driver (30kHz).

The quadrant sensing elements are being used in the photovoltaic mode with feedback resistors of 88.7k ohms. The value of the feedback resistor was determined by studying the losses of power throughout the system. See figure 13 for a list of the

calculations involved in determining these losses. The initial power out of the laser is 3mW. The modulation duty cycle of the laser driver is 40%, which means that the power out is reduced to 1.2mW. The beam expander optics have a transmission of 92%, and atmospheric absorption is approximately 2% which yield a power of 1.08mW reaching the reducer optics. The interference filter on the front of the reducer has a transmittance of 60% which reduces the power to .65mW into the reducer lenses. The beam reducer lenses have a transmission of 92%, and the glass cover of the quadrant detector has a transmission of 92%. The final power incident onto the detector is 0.55mW.

1) $\phi_{laser} = 3$ mW typical

2) Laser modulation duty cycle = 40 percent

$\phi_{out} = .4 \, (3 \text{ mW}) = 1.2 \text{ mW}$

3) Beam expander : 4 surfaces with MgF coating

$T = (1 - .02)^4 = 92$ percent

$\phi_{out} = .92 \, (1.2 \text{ mW}) = 1.1 \text{ mW}$

4) Atmospheric Absortion = 2 percent

$T = 98$ percent

$\phi_{out} = .98 \, (1.1 \text{ mW}) = 1.08 \text{ mW}$

5) Interference filter : T specified = 60 percent

$\phi_{out} = .60 \, (1.08 \text{ mW}) = 0.65 \text{ mW}$

6) Beam reducer : 4 surfaces with MgF coating, $R = 2$ percent

$T = (1 - .02)^4 = 92$ percent

$\phi_{out} = .92 \, (.65 \text{ mW}) = 0.60 \text{ mW}$

7) Glass cover of quadrant detector : 2 surfaces, $R = 4$ percent

$T = 92$ percent

$\phi_{out} = .92 \, (.60 \text{ mW}) = 0.55 \text{ mW}$

Figure 13. System losses

it is treated as a dc offset signal. Therefore to remove the dc offset from the modulated signal it is capacitively coupled to the synchronous detector. Each of the four quadrant outputs is fed into a synchronous detector. The synchronous detector transforms the ac modulated signal back to a dc level. A low pass filter is then used at the output of the synchronous detector to filter out the spikes due to any timing errors generated by the CMOS switches. The output of the low pass filter is then input to the non-inverting unity gain op amps so that the summing and differencing amplifiers will not be affected by the impedance of the filter. Opposing quadrant outputs are arranged so that one channel contains A and C, while the other channel contains B and D. These output pairs are then fed into summing and differencing amplifiers. The outputs of the summing and differencing op amps are then fed into the numerator and denominator inputs (respectively) of an integrated circuit divider. The output of the divider is given by: 10*(NUM/DEN), which results in a voltage swing of +10V to -10V. The divider output is used as the system output.

RESULTS

The system was tested using an enclosed 8 story vertical test tower approximately 150 feet (46 meters) in length. The test set up is shown in figure 15. The system was aligned by retroreflecting the laser from a mirror placed in front of the reducer optics in place of the interference filter. The tilt stage that the laser/expander assembly was mounted to was adjusted until the laser beam was reflected back onto the laser. After the system was aligned, the mirror was replaced with the interference filter.

Data was taken by translating the reducer/detector assembly in one direction with small increments (.015 inches) while tracking the output voltage from the divider. The resulting plots of voltage vs. position are shown in figure 16. The graphs show that the central portion of the quadrant detector has a linear response of .008 inches per volt. The detector response is approximately parabolic at the outer regions of the travel range. This response is expected, and does not inhibit the system performance in a nulling application. By studying the graphs, it can be determined that the linear travel range is approximately .15 inches (4 mm) in both axes.

The critical requirement on this system is that it must have a resolution of better than 100 microns at 50 meters. The resolution was checked by attaching a strip chart recorder to one of the system output channels and adjusting the translation stages until the outputs on both channels were near zero. One translation stage was then moved a known amount in order to calibrate the strip chart response. Then, the stage was moved back to its original position and the system response was monitored for approximately 1 minute on the strip chart recorder. See figure 17 for the strip chart
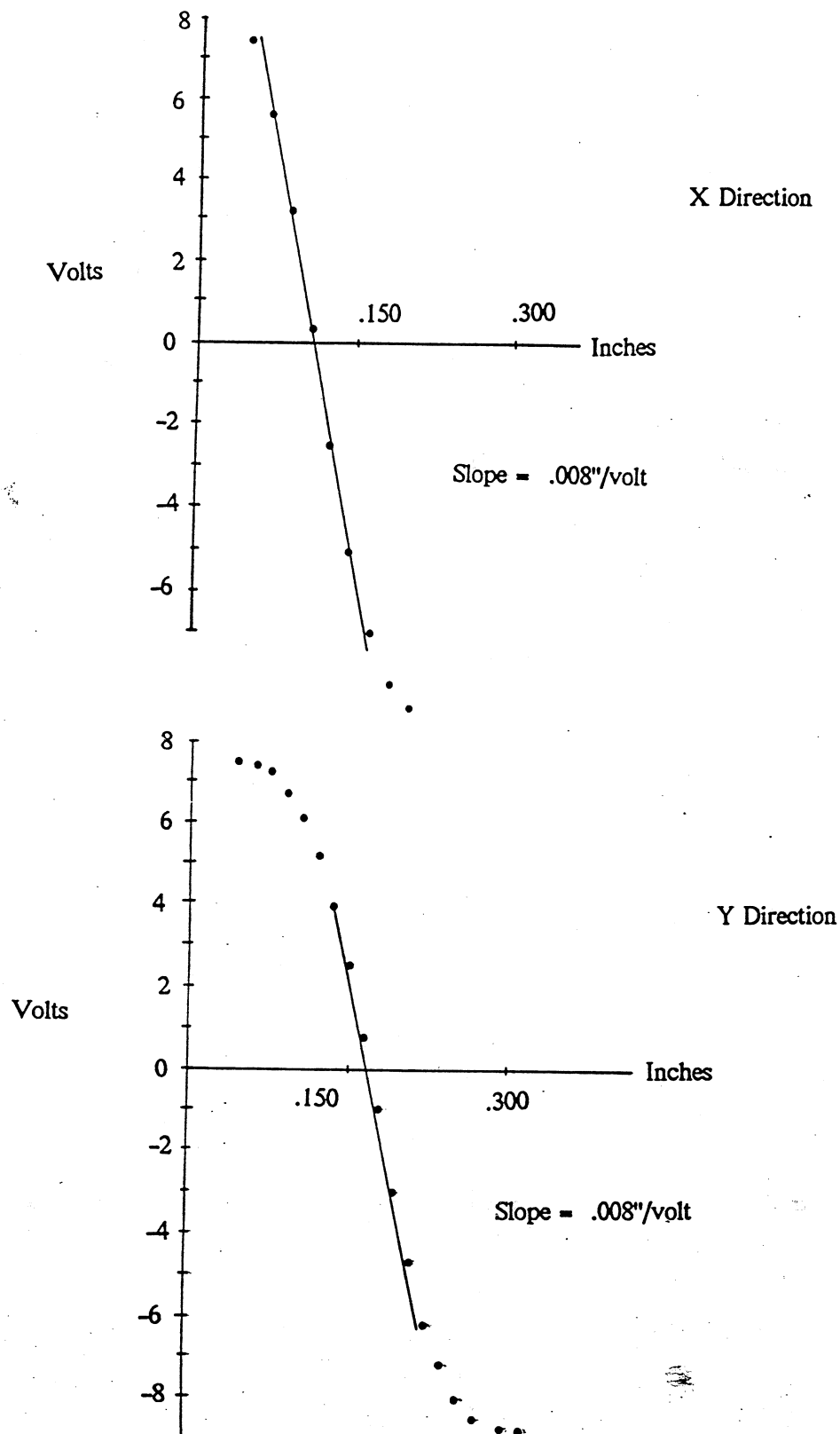
X Direction

Volts

Inches

.150   .300

Slope = .008"/volt

Y Direction

Volts

Inches

.150   .300

Slope = .008"/volt

Figure 16. Voltage vs. Position

Appendix B
Example Output of Program qd

At QD rigging elevation 44.0 degrees:

(Coordinates in EL coordinate system)
Laser node   1000: Location - 0.000, 0.000, 0.000
            Displacement - 0.000, 0.197, 0.148
            Tilt - -0.0002, 0.0000, 0.0000

Det node 40710: Location - 0.000,-2130.940,2135.560
            Displacement - 0.000, 3.310, 0.824
            Tilt - 0.0000, 0.0000, 0.0000

Laser Beam length at rigging: 3015.1538

Laser position in elevation coordinate system:

| | Absolute | | | Rel to rigged | | |
EL	X	Y	Z	X	Y	Z
0	0.000	0.355	0.659	0.000	0.158	0.510
5	0.000	0.356	0.593	0.000	0.159	0.445
10	0.000	0.352	0.528	0.000	0.155	0.380
15	0.000	0.343	0.464	0.000	0.145	0.316
20	0.000	0.329	0.403	0.000	0.131	0.255
25	0.000	0.310	0.344	0.000	0.113	0.196
30	0.000	0.286	0.287	0.000	0.089	0.139
35	0.000	0.258	0.234	0.000	0.061	0.086
40	0.000	0.226	0.185	0.000	0.029	0.037
45	0.000	0.190	0.139	0.000	-0.008	-0.009
50	0.000	0.150	0.098	0.000	-0.048	-0.050
55	0.000	0.106	0.062	0.000	-0.091	-0.086
60	0.000	0.060	0.031	0.000	-0.138	-0.117
65	0.000	0.010	0.005	0.000	-0.187	-0.144
70	0.000	-0.042	-0.016	0.000	-0.239	-0.164
75	0.000	-0.095	-0.031	0.000	-0.293	-0.180
80	0.000	-0.151	-0.041	0.000	-0.348	-0.189
85	0.000	-0.207	-0.045	0.000	-0.404	-0.193
90	0.000	-0.264	-0.043	0.000	-0.462	-0.191

Appendix B - Example Output of Program qd

Detector position in elevation coordinate system:

		Absolute			Rel to rigged	
EL	X	Y	Z	X	Y	Z
0	0.000	-2122.759	2138.754	0.000	4.871	2.370
5	0.000	-2123.121	2138.468	0.000	4.508	2.083
10	0.000	-2123.541	2138.181	0.000	4.089	1.797
15	0.000	-2124.015	2137.896	0.000	3.614	1.511
20	0.000	-2124.540	2137.614	0.000	3.089	1.230
25	0.000	-2125.112	2137.339	0.000	2.518	0.955
30	0.000	-2125.726	2137.072	0.000	1.904	0.688
35	0.000	-2126.378	2136.815	0.000	1.252	0.431
40	0.000	-2127.062	2136.570	0.000	0.568	0.186
45	0.000	-2127.774	2136.339	0.000	-0.144	-0.045
50	0.000	-2128.508	2136.124	0.000	-0.878	-0.260
55	0.000	-2129.259	2135.927	0.000	-1.629	-0.458
60	0.000	-2130.020	2135.748	0.000	-2.390	-0.637
65	0.000	-2130.787	2135.589	0.000	-3.157	-0.795
70	0.000	-2131.552	2135.452	0.000	-3.922	-0.932
75	0.000	-2132.311	2135.338	0.000	-4.681	-1.047
80	0.000	-2133.058	2135.246	0.000	-5.428	-1.138
85	0.000	-2133.786	2135.179	0.000	-6.156	-1.205
90	0.000	-2134.491	2135.137	0.000	-6.861	-1.248

Laser beam tip position in elevation coordinate system:

		Absolute			Rel to rigged	
EL	X	Y	Z	X	Y	Z
0	0.000	-2126.800	2137.563	0.000	0.829	1.179
5	0.000	-2126.844	2137.454	0.000	0.786	1.069
10	0.000	-2126.901	2137.336	0.000	0.729	0.951
15	0.000	-2126.973	2137.210	0.000	0.657	0.826
20	0.000	-2127.058	2137.078	0.000	0.572	0.694
25	0.000	-2127.156	2136.940	0.000	0.474	0.556
30	0.000	-2127.265	2136.798	0.000	0.364	0.413
35	0.000	-2127.387	2136.652	0.000	0.243	0.268
40	0.000	-2127.518	2136.504	0.000	0.112	0.119

45	0.000	-2127.659	2136.354	0.000	-0.029	-0.030
50	0.000	-2127.808	2136.205	0.000	-0.178	-0.179
55	0.000	-2127.964	2136.056	0.000	-0.334	-0.328
60	0.000	-2128.126	2135.910	0.000	-0.496	-0.474
65	0.000	-2128.292	2135.767	0.000	-0.662	-0.617
70	0.000	-2128.462	2135.629	0.000	-0.832	-0.756
75	0.000	-2128.634	2135.495	0.000	-1.005	-0.889
80	0.000	-2128.807	2135.369	0.000	-1.177	-1.016
85	0.000	-2128.980	2135.249	0.000	-1.350	-1.135
90	0.000	-2129.150	2135.138	0.000	-1.520	-1.246

Laser beam tip position in L2 coordinates:

	Absolute		
EL	X	Y	Z
0	-0.000	-0.000	3015.154
5	-0.000	0.000	3015.154
10	-0.000	0.000	3015.154
15	-0.000	0.000	3015.154
20	-0.000	0.000	3015.154
25	-0.000	0.000	3015.154
30	-0.000	-0.000	3015.154
35	-0.000	0.000	3015.154
40	-0.000	0.000	3015.154
45	-0.000	0.000	3015.154
50	-0.000	0.000	3015.154
55	-0.000	0.000	3015.154
60	-0.000	0.000	3015.154
65	-0.000	-0.000	3015.154
70	-0.000	0.000	3015.154
75	-0.000	0.000	3015.154
80	-0.000	0.000	3015.154
85	-0.000	0.000	3015.154
90	-0.000	-0.000	3015.154

Detector position in L2 coordinates:

Absolute

Appendix B - Example Output of Program qd

EL	X	Y	Z
0	-0.000	-3.705	3013.147
5	-0.000	-3.353	3013.246
10	-0.000	-2.977	3013.382
15	-0.000	-2.579	3013.553
20	-0.000	-2.162	3013.758
25	-0.000	-1.730	3013.995
30	-0.000	-1.284	3014.262
35	-0.000	-0.830	3014.558
40	-0.000	-0.370	3014.879
45	-0.000	0.092	3015.225
50	-0.000	0.553	3015.591
55	-0.000	1.009	3015.976
60	-0.000	1.457	3016.376
65	-0.000	1.893	3016.789
70	-0.000	2.313	3017.210
75	-0.000	2.716	3017.638
80	-0.000	3.097	3018.068
85	-0.000	3.453	3018.498
90	-0.000	3.783	3018.923

DETECTOR NODE [40710]
0, -2130.9399, 4035.3601 (Cent Front Top Rx Room)

FOCUS

QD-BORESIGHT 2

VERTEX

0, -78,960, 2079,3601
(Top Box directly above cen
El shaft, 191,21" above)

FIGURE 1

GBT view showing the QD laser beam.

FIGURE 2

Cross-section through the backup
and box structure identifying
three possible locations for the
QD laser.
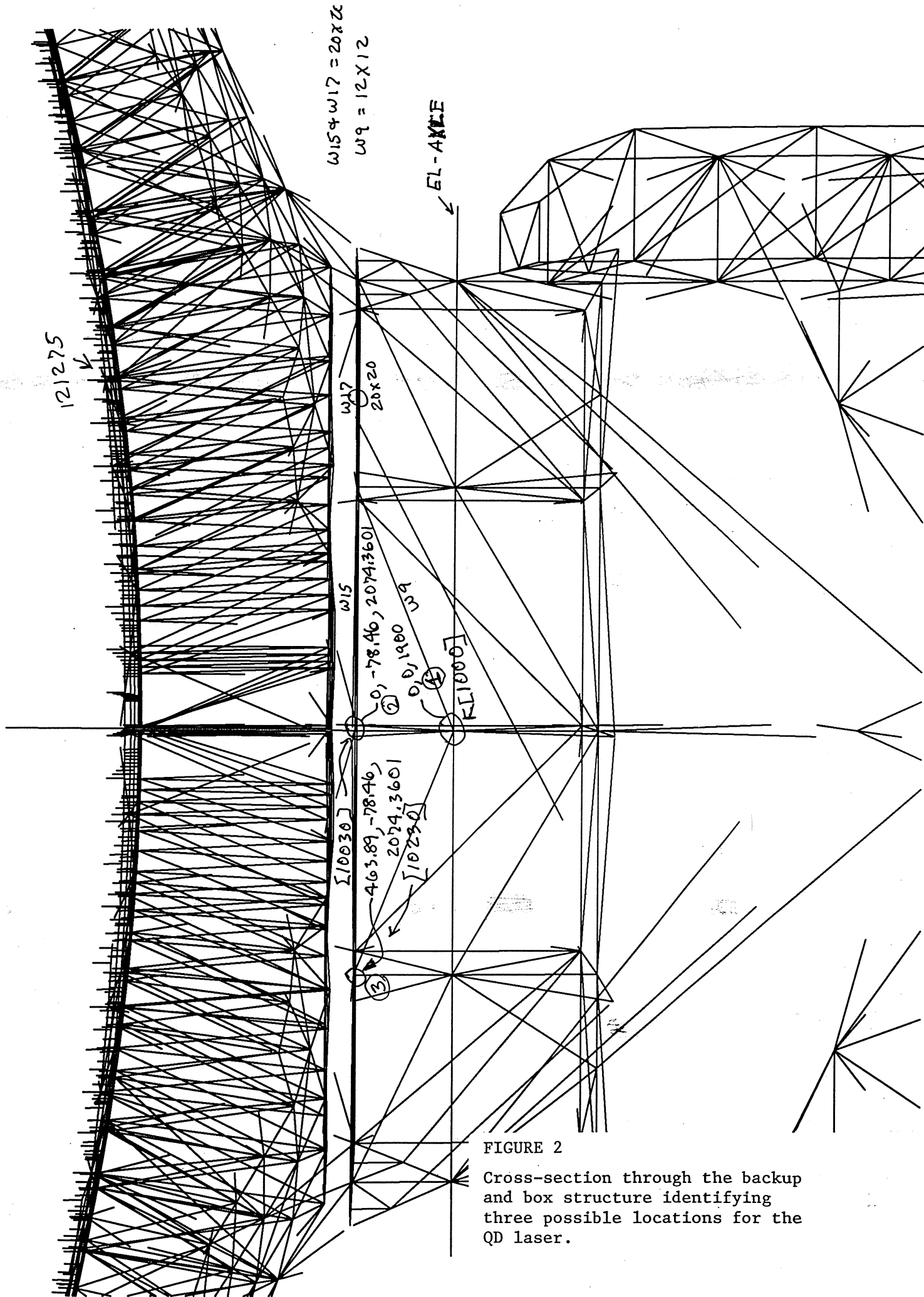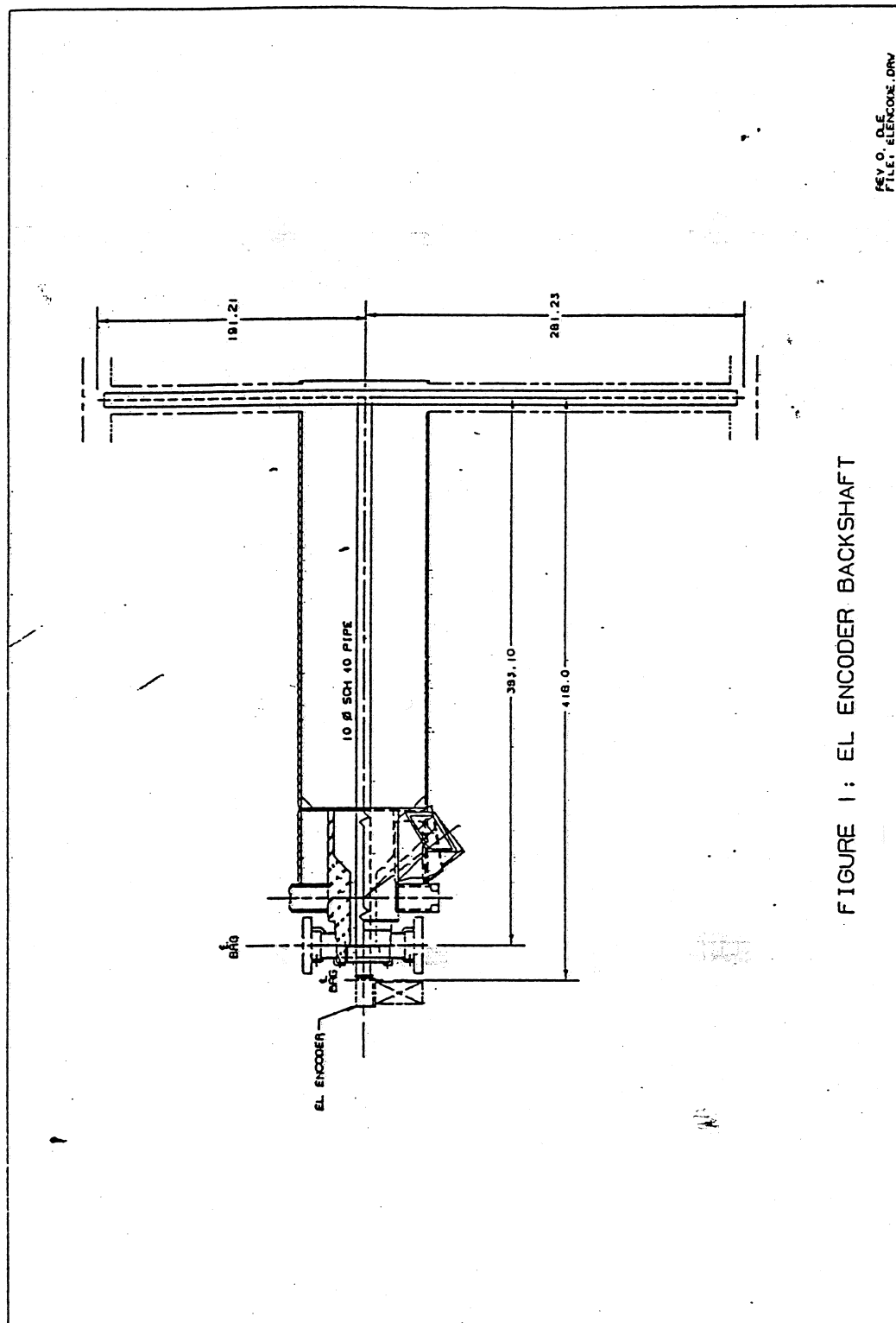
FIGURE 1: EL ENCODER BACKSHAFT

FIGURE 3

The elevation encoder backshaft.

5

VIEW QUAD-BORESIGHT
PERSPECTIVE FROM N1000
CEN OF EL SHAFT
(0,0,1900)

1+17

FIGURE 4

Prespective AUTOCAD view from
node 1000.
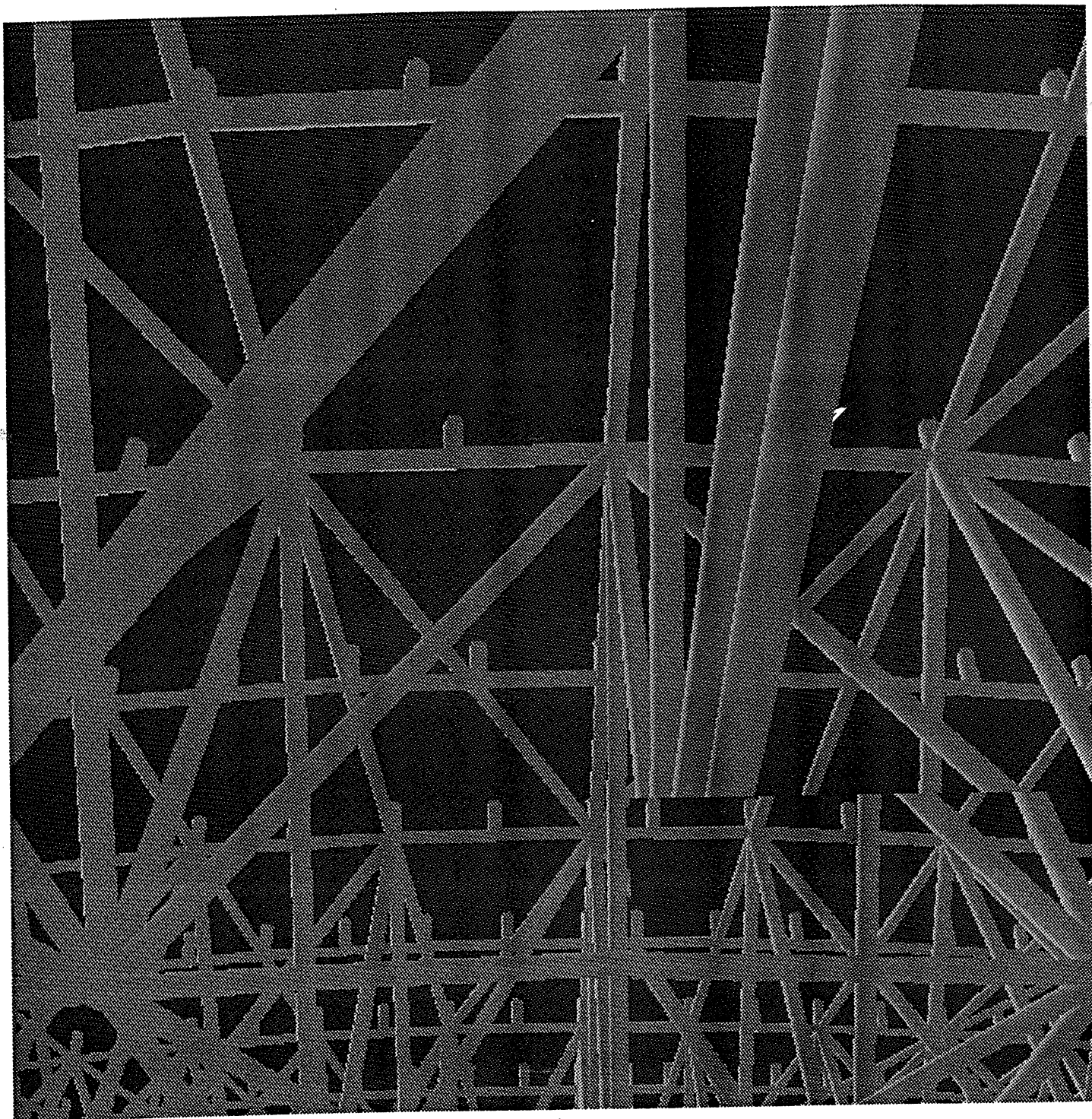
From (30, 0, 1900) to (0, -2131, 4035)

Case 1

From N 1000

FIGURE 5

View from near near node 1000.
Members of the backup and box
structure are represented by
four inch tubes.

VIEW QD-BORESIGHT 2
FROM NODE 10030.

PERSPECTIVE VIEW
FROM TOP OF BOX
DIRECTLY OVER
CEN EL SHAFT
QD POS ②
(0, -78.46, 2074.360 1)

H-17

FIGURE 6

AUTOCAD perspective view from
node 10030.
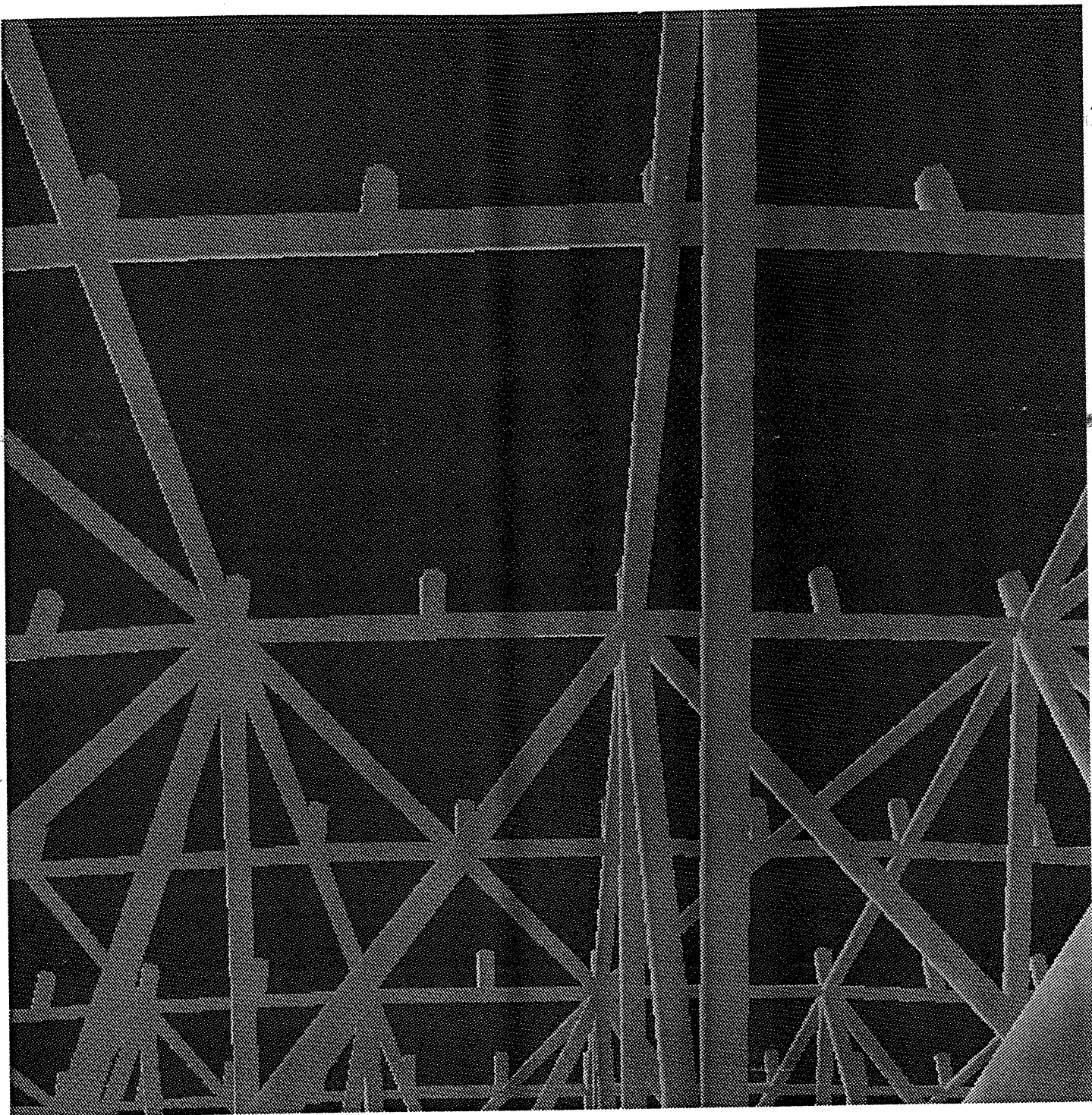
file rnorrod 951005 c.ps   Case 2

From (30, -78.5, 2074.4) to (0, -2131, 4035)

F. Clip 20.

FIGURE 7

View from near node 10030.
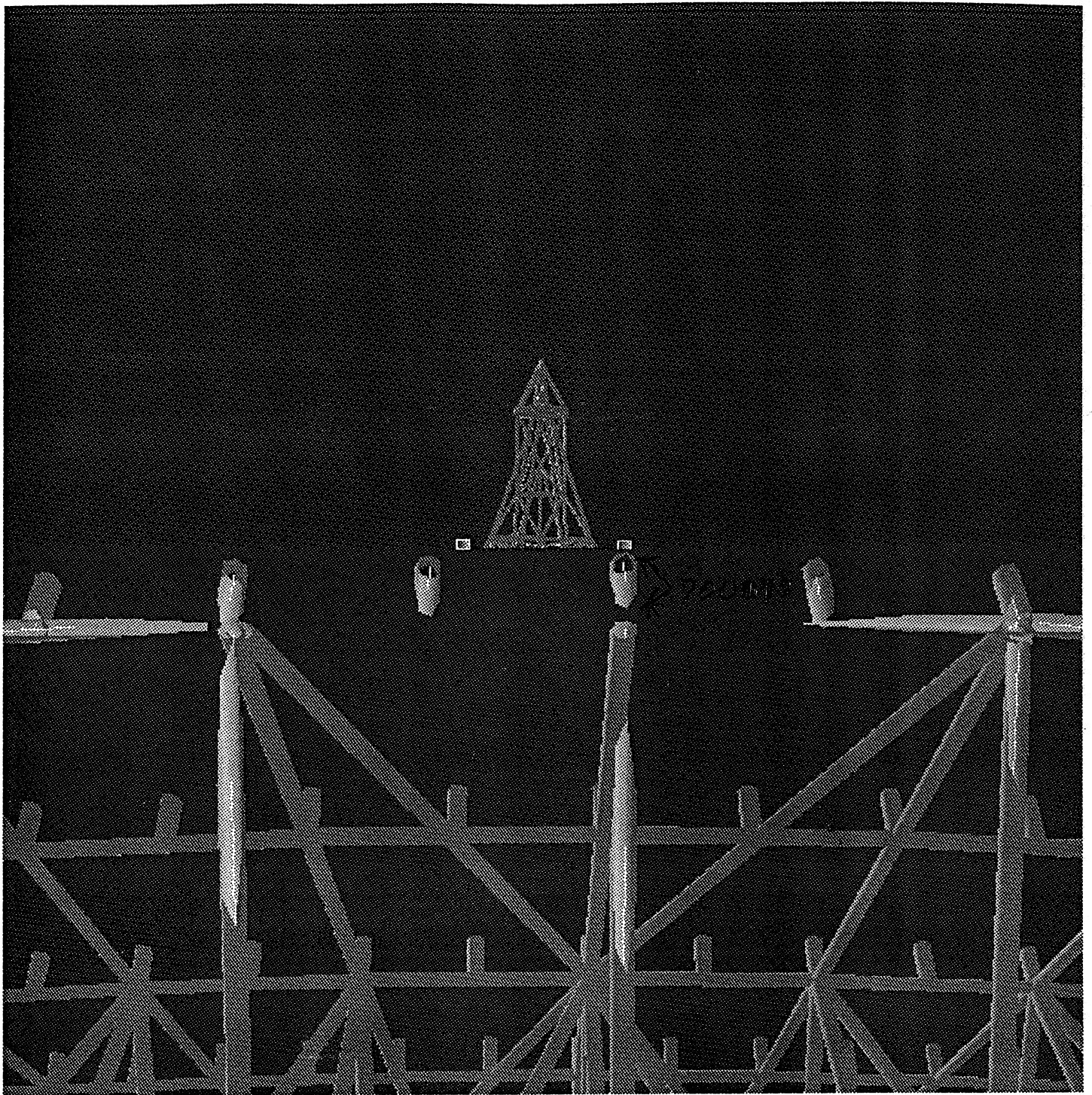
Actuator 700017 @ 0, -436.61, 2410.44

rnorrod957005b.ps
   Camera @ (0, -78.5, 2074.4) to (0, -2130.9, 4035.56)
   Clip @ 490" (from camera)   CASE 2

FIGURE 8

Similar to Figure 7.
A clipping plane along the line
of sight allows viewing of the
feedarm.

QD Case 2

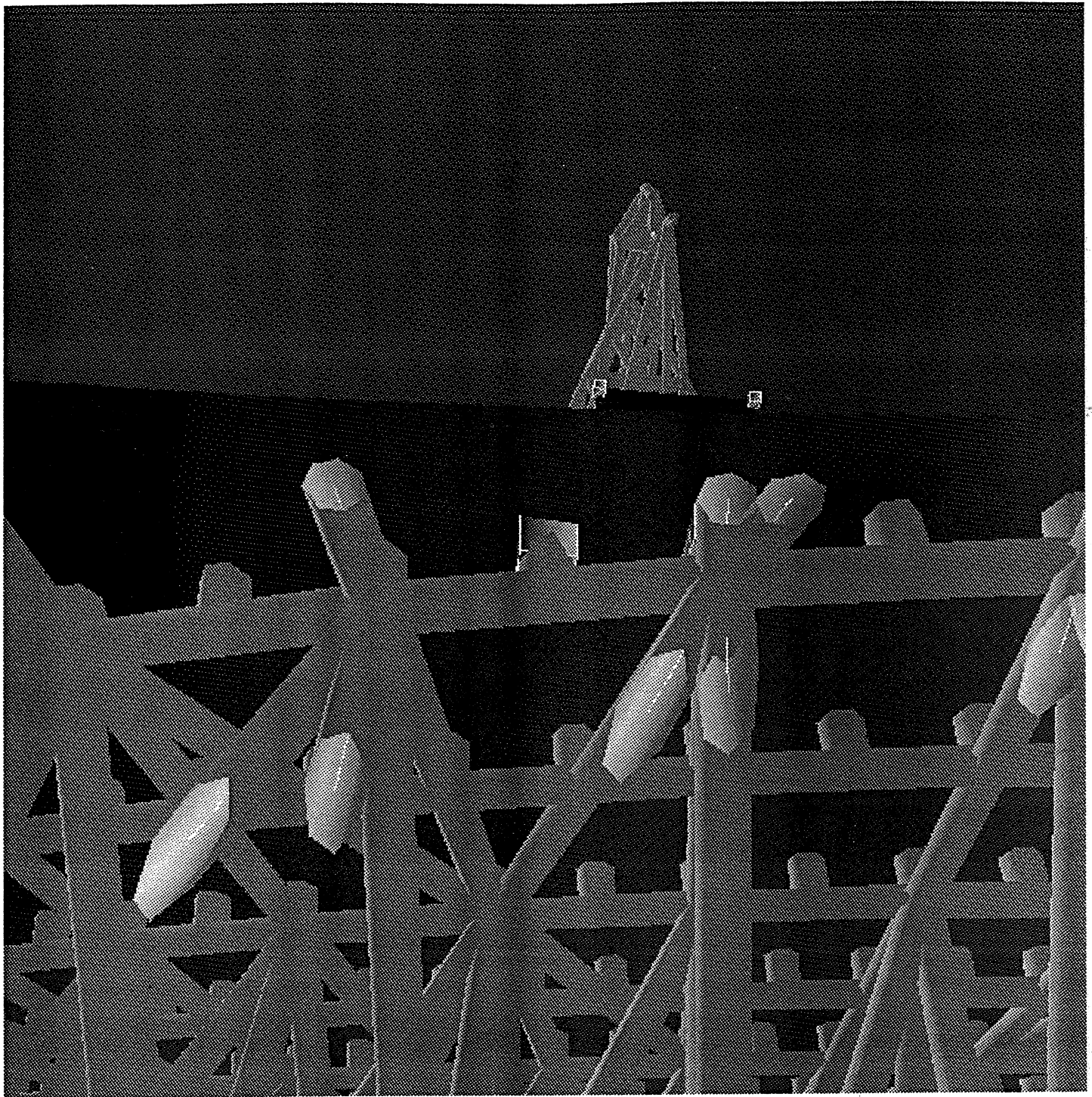Detector Position in L2
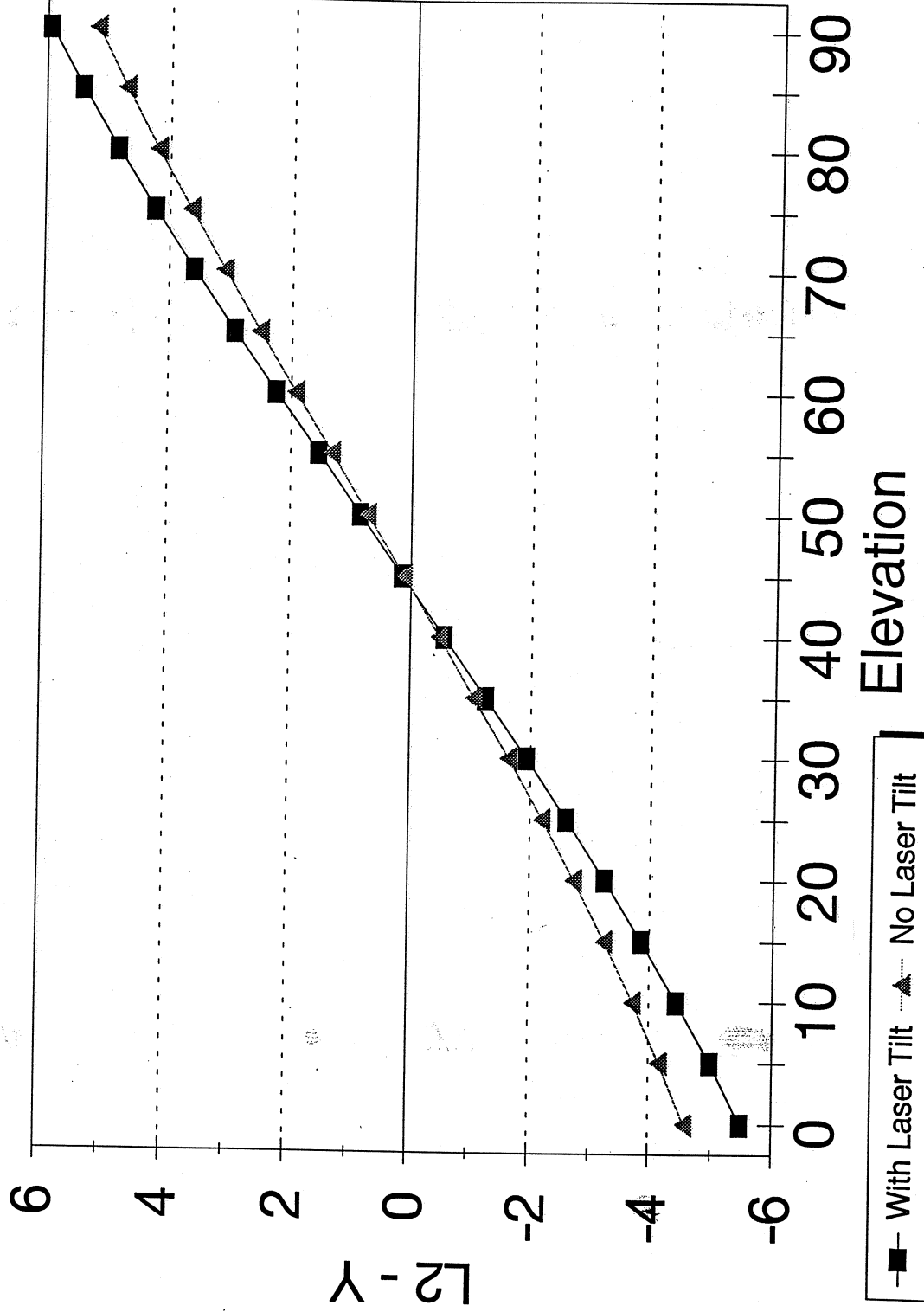
FIGURE 9

Perspective View
From QD pos ③
NODE 10230

7/2018

7/2018

714018
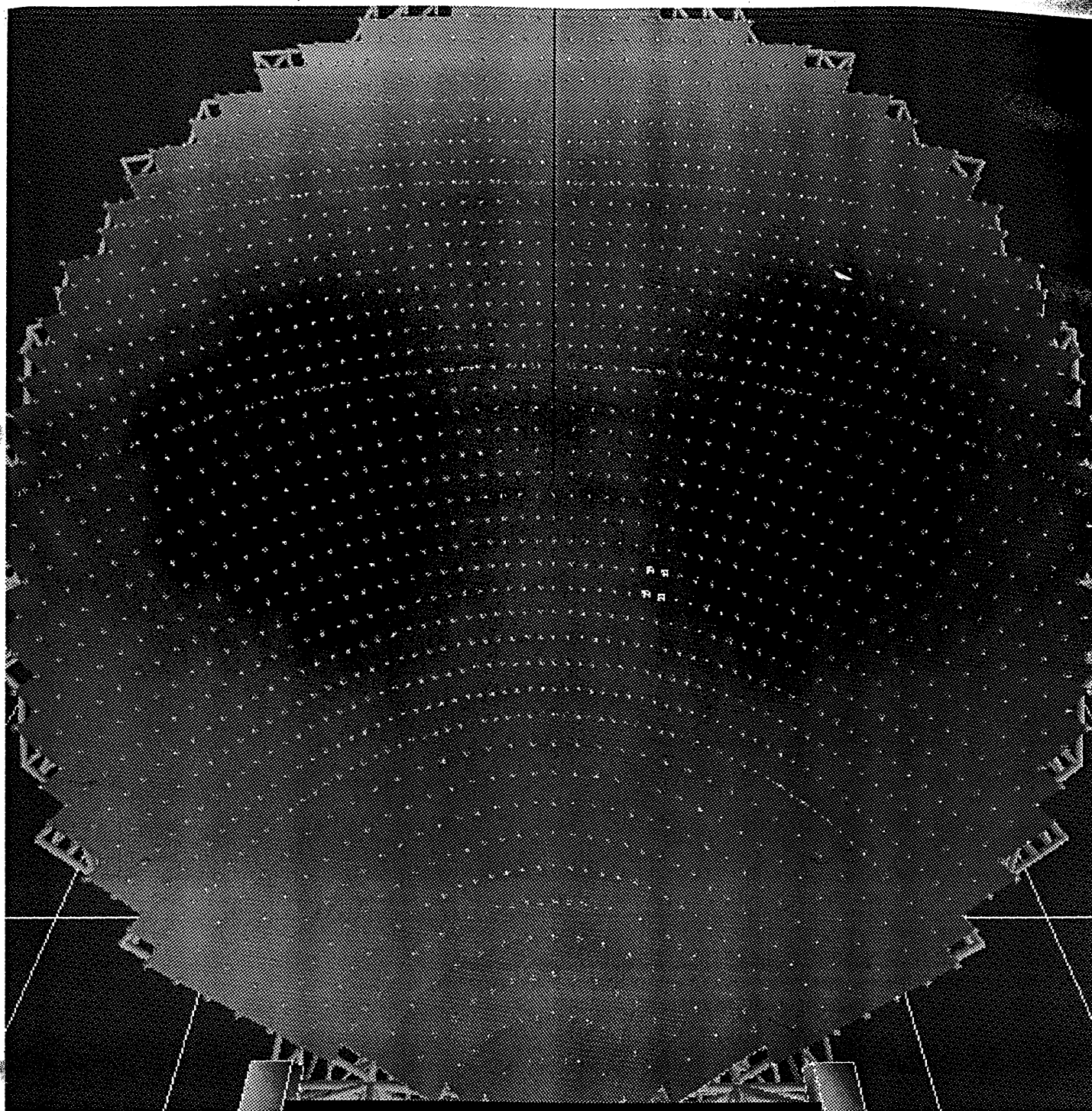
#714017
(419-489, 2410)

FIGURE 10

AUTOCAD perspective view from
node 10230.

From (464, -78, 2094) to (419, -489, 2410)
10" DIA MEMBERS

FIGURE 11

View from near node 10230.
Backup members are represented
by 10 inch tubes.

From $(0, -2159, 4459)$ "P.F." to $(0, -304, 2421)$ "Along feed boresight"

FOV: 780 UP vector $[0, .740, .673)$

FIGURE 12

The highlighted panel lies between hoops 17 and 18. A laser beam from 10230 goes through this panel.

ACKNOWLEDGEMENTS

REFERENCES

[1] P. Goldsmith, "Quasi-Optical Techniques at Millimeter and Submillimeter Wavelengths," Infrared and Millimeter Waves, Vol. 6, Academic Press, 1982.

[2] UDT Instruments, A Guide to Position Sensing, p.2, 1991.

[3] UDT Instruments, p.1.

[4] H. Weichel, Laser Beam Propagation in the Atmosphere, SPIE Optical Engineering Press, 1990, pp.61-63.

[5] H. Weichel, p.22.

[6] T. Chiba, "Spot Dancing of the Laser Beam Propagated Through the Turbulent Atmosphere," Appl. Opt. 10, 2456 (Nov. 1971).

[7] H. Weichel, p.49.